A new test methodology based on structural resonance for mode I fatigue delamination growth in an unidirectional composite

Irène Maillet, Laurent Michel, Germain Rico, Mathieu Fressinet, Yves Gourinat

A new test methodology based on structural resonance for mode I fatigue delamination growth in an unidirectional composite

I. Maillet [a,*], L. Michel [a,**], G. Rico [b], M. Fressinet [b], Y. Gourinat [a]

[a] Université de Toulouse, INSA, UPS, Mines Albi, ISAE, ICA (Institut Clément Ader), 10 av. Edouard Belin, BP 54032, 31055 Toulouse, France
[b] DGA Techniques Aéronautiques, 47 rue St. Jean, BP 93123, 31131 Balma, France

Keywords:
Fiber reinforced polymer matrix
Delamination resistance
Mode I loading
Resonance test development
Vibratory fatigue
Frequency effect

A B S T R A C T

A specific device has been set up to test by vibration resonance the mode I fatigue delamination growth onset of composite laminates. This test system, based on the DCB test specimen, is a mass-spring-specimen dynamic system designed to resonate. The defined operating conditions allow performing delamination propagation tests under imposed load and stopping the test under reproducible conditions, identical to the ones recommended in the ASTM-D6115 standard. This system allows fatigue tests to be driven up to 100 Hz, reducing the time taken by a factor of ten without detrimental heat being generated in the material. The effect of frequency on the fatigue delamination growth on mode I has been investigated through a comparison with standard tests performed at 10 Hz. A decrease in resistance to the propagation of delamination is observed with the increase in frequency for the composite studied. This frequency effect seems to be a strain rate effect and was taken in consideration by using dynamical critical energy restitution rate for the *G–N* curve plotting.

1. Introduction

Due to their lightness and stress adaptability, composite materials are more and more used in the aeronautical frame. Aeronautical structures are submitted to vibrations during their service life due to aerodynamic turbulent flow around the structure. In this sonic fatigue domain applied loads remain low, but performed at high frequency a great number of cycles can be reached within a short time [1]. Damage tolerance policy should address any risk of delamination propagations within the whole service life of airplanes [2]. Even if the sonic fatigue case is not the major design problem, investigation of knowledge of composite material behavior under high cycle fatigue seems to be of sufficient importance to be addressed.

A delamination will propagate under a combination of the three pure modes: opening mode (mode I), sliding mode (mode II) and tearing mode (mode III). Pure modes I and II tests are generally used to characterize composite material in fatigue [3–6]. For the more critical mode, the mode I, the ASTM defined the Double Cantilever Beam (DCB) test as a standard [3]. This DCB fatigue test is achieved at a frequency of 10 Hz, with a controlled loading ratio and a test stop condition linked to the specimen compliance. Then fatigue behavior of carbon/epoxy laminate in pure mode I up to 10^6 cycles has been widely studied [7,6,8]. At this frequency the duration of test needed to reach 10^6 cycles is more than 11 days. In these conditions exploration of the high cycle fatigue field cannot be considered. Indeed delamination propagation under pure mode of composite material laminates at high frequency to reach high cycle fatigue still seems not to be addressed in the literature.

In the frame of accelerated fatigue tests, new test methodologies were developed in order to increase frequency of tests, applied mainly for metallic materials. George et al. [9] designed vibration fatigue test under resonance conditions to represent uni-axial and bi-axial bending loadings of turbine blades. They used a finite element model to design a suitable plate specimen and tested it to determine the endurance limit with the Maxwell and Nicholas method [10]. In this method, the specimen is loaded by stress steps, each step corresponding to the number of cycles of the estimated endurance limit (around 10^6 cycles). The tests are performed on a shaker at frequencies around 1000 Hz, and at a stress ratio of -1, allowing to reach 10^6 cycles within a few hours. Bathias [11,12] developed a piezoelectric fatigue machine working at 20 kHz or 30 kHz for tension–compression test and three-point bending test at different loading ratios. Those tests are mostly used to observe the metallic behavior in gigacycle fatigue in different environment conditions [13–15].

For organic matrix composite materials mechanical behavior is very sensitive to frequency. Frequency effects can be divided in

* Corresponding author. Tel.: +33 (0) 561339195; fax: +33 (0) 561339095.
** Principal corresponding author. Tel.: +33 (0) 561339141; fax: +33 (0) 561339095.
E-mail addresses: irene.maillet@isae.fr (I. Maillet), laurent.michel@isae.fr (L. Michel).

three competitive parts [16,17]: a creep effect in the low frequency domain (below 10 Hz), a strain rate effect in the high frequency domain and the self generated heating due to the low thermal conductivity of the material most likely to appear at elevated loading frequencies.

Wang et al. [18] used a piezoelectric ultrasonic fatigue machine to test in gigacycle regime crack growth in bonded composite repairs of notched metallic plates as a function of the number of patch plies. The patches were in boron-epoxy and their ability to delay the crack propagation in a notched aluminum alloy specimen was investigated. No mention of temperature observation during tests was reported despite the very high load frequency.

Other authors were interested in high cycle fatigue of composite material. Michel et al. [19] studied the AS4/PEEK in tension, compression and bending. For tension and compression tests:

- on hydraulic test machine for low and medium cycle fatigue test in the frequency range of 0.5–10 Hz, and
- on electromechanical resonance machine for high cycle and gigacycle regime in the range of 57–158 Hz. These tests were conducted at room temperature with a cooling air flow allowing the specimen surface temperature to remain below 45 °C.

Three-points bending tests were performed with the help of a servo-hydraulic actuator between 0.5 Hz and 10 Hz for low cycle regimes and at 50 Hz for high ones without cooling system.

In this study for most of the tests the material fatigue behavior was found to follow a log linear law independent of the frequency: results for high frequency ranges were consistent with the ones at low frequencies. For pure compression case, results seem however to be sensitive to frequency. Although the specimen temperature during tests remained far below the glass temperature of the PEEK matrix, the authors assigned this behavior to a local buckling of fibers due to the temperature induced softening of the matrix. Hosoi et al. [20,21] investigated the influence of transverse cracks on delamination initiation and propagation in CFRP during tensile fatigue test. All the tests were conducted with an hydraulic testing machine. For high cycle fatigue, the test frequency was 100 Hz with low applied load to limit the temperature rise to 10 °C. Within this condition the authors ensured there was no temperature effect in their results.

The aim of this work is then to implement a suitable test methodology to investigate the mode I propagation threshold for a large number of cycles. As the DCB specimen is loaded under bending, it requires consequent displacements: a minimum displacement of 1 mm for the Energy Restitution Rate range tested in our study. As it is difficult to reach at the same time high frequency and large displacement with classical machines, an accelerating testing device has been designed and fixed on a shaker. The device principle is based on resonance of mass-spring-specimen system and allows to perform tests at 100 Hz, hence reducing the time taken by a factor of ten, as compared to conventional tests. A standard CFRP laminate widely used in aeronautical domain is then characterized with the new apparatus and the results compared with a classical characterization: at medium frequency (10 Hz).

2. Classical characterization

2.1. Material specimen and facilities

Specimens used are unidirectional composite beams made of 20 plies of T700/M21 (Hexcel©). The beam specimens were cut out from a press manufactured plate. The curing cycle followed a standard cycle with an homogenization stage as recommended by Hexcel©. A 25 μm thickness Teflon film is inserted in the midplane of the laminate during the manufacturing to create an initial crack. It is larger than the standards' recommended 13 μm [22], but all the specimens were pre-cracked in mode I loading to get at least a 2 mm delamination extension before the fatigue tests.

The specimen dimensions conform to the standard ASTM D5528 [22] of the delamination propagation test in mode I ($L = 180$ mm, $b = 25$ mm, $h = 2.5$ mm, $a_0 = 50$ mm Fig. 1) It is instrumented with a RUMUL© crack gauge to follow the crack propagation during tests. The load is applied by the means of loading blocks stuck on both sides of the specimen. The loading block section dimension is 10×10 mm^2. (Fig. 2).

The tests were performed on a servo-hydraulic machine equipped with a 1 kN load–capacity cell. The parameters measured and used for the data reduction were the opening displacement, the crack extension and the load.

2.2. Specimen compliance law and resistance

Preliminary mode I interlaminar fracture toughness tests were conducted for various crack sizes to determine the propagation values of fracture toughness G_{Ip} and the master compliance curve of the specimen. This curve links the specimen stiffness to the delamination size.

The static compliance law is then (Fig. 3).

$$C = C_0 \cdot a^n \tag{1}$$

where C is the compliance and a is the measured crack length: $C_0 = 4.28\ e^{-7}$ and $n = 2.83$

Some authors found that carbon/epoxy materials are rate sensitive [23]. In order to investigate loading rate effects on the Energy Restitution Rates (ERR) in pure mode I, several tests where performed. The cross head speed was controlled at 0.01 mm/s (following the ASTM standards) for four specimens and at higher speeds for others (from 5 mm/s to 150 mm/s).

The ERR is calculated with the compliance method (Eq. (2)) [22].

$$G = \frac{nP\delta}{2ba} \tag{2}$$

where G is the ERR, P the load, δ the opening displacement and b the width of the specimen.

All the specimens were found to follow the same compliance law (Fig. 3 on the left). After analyze two distinct propagation energy restitution rates in mode I are found: $G_{I_p^{sta}} = 400$ N/m for the lower loading rates and $G_{I_p^{dyn}} = 300$ N/m for higher ones (Fig. 3 on the right).

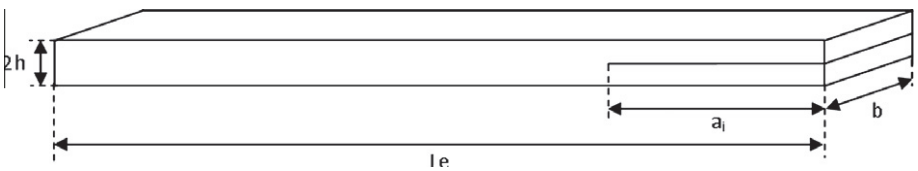

Fig. 1. Specimen geometry.

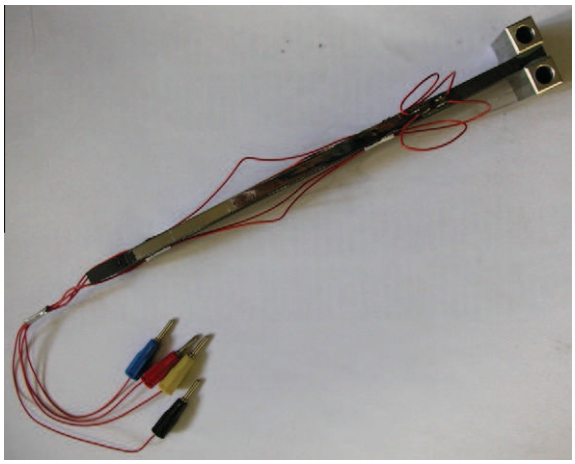

Fig. 2. Test specimen according to ASTM D5528 with electrical crack gauge.

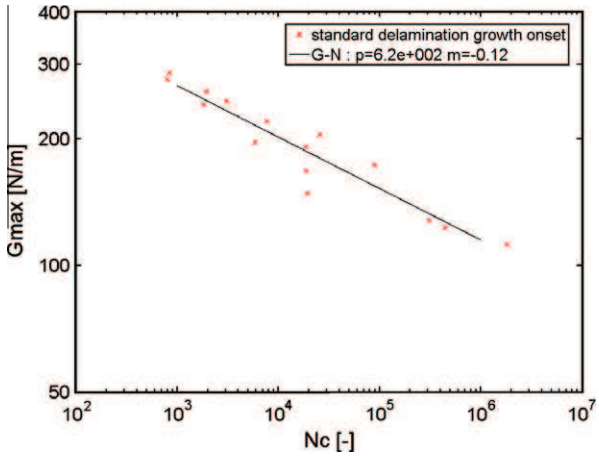

Fig. 4. *G–N* onset propagation curve at 10 Hz and $R = 0.1$.

2.3. Classical DCB fatigue test

2.3.1. Test conditions

DCB fatigue tests have been performed at a controlled displacement ratio of $R = 0.1$ and a frequency of 10 Hz following the standard requirements [3].

2.3.2. Data reduction

The fatigue compliance is assumed to follow the static compliance law (Eq. (1)). The ERR is then calculated with the compliance method (Eq. (3)) [22].

$$G_{max} = \frac{nP_{max}\delta_{max}}{2ba} \tag{3}$$

where G_{max} is the maximal ERR reach during a cycle, P_{max} the maximal load and b the width of the specimen.

G–N curve. Six specimens were used to determine the *G–N* onset propagation curve which links the ERR and the number of cycles to the propagation onset.

The *G–N* curve is then plotted and the parameters determined (Fig. 4):

$$G_{max} = p \cdot N_c^m \tag{4}$$

where N_c is the number of cycles necessary to reach the propagation threshold value. It is defined as the number of cycles until the compliance has increased by 5% by the ASTM D6115 [3].

Although this method is the one recommended by the ASTM, most of the authors used the Paris law to characterize delamination propagation in fatigue. Brunner et al. [4] even proposed a new standardized procedure of interlaminar delamination propagation in mode I to take this into account.

Paris law. Three specimens were used to identify the relation between the crack speed $\left(\frac{da}{dN}\right)$ vs the ERR (G): the Paris law (Eq. (5)). It has been chosen to use dimensionless value by dividing ERR by the propagation ERR $\left(G_{Ip}^{stat}\right)$.

$$\frac{da}{dN} = k\left(\frac{G_{max}}{G_{Ip}^{stat}}\right)^n \tag{5}$$

where N is the number of cycles.

The Paris curve obtained presents a classical linear variation with deviations for the highest and lowest ERR ratios of the testing range (highlighted by dashed lines on the graph 5). A no propagation threshold can be estimated around 140 ± 15 N/m taking into account the measurement accuracy.

Results from the different specimens clearly follow a Paris law which is then found to be independent of the propagation length (Fig. 5). It should be noted that this length necessary to cover the whole range of Paris curve is fairly limited: no more than 22 mm. With this short crack extension, no fiber bridging was observed during fatigue tests. Any change in compliance is then directly linked to the delamination extension rather than to any process zone increase.

So the *G–N* onset propagation curve can be extrapolated from the Paris test results by dividing the total propagation into segments, each one linked to one propagation threshold. The number of cycles used to determine the threshold value is defined as the number of cycles until the compliance has increased by 5% as it was used for the test before (Fig. 5).

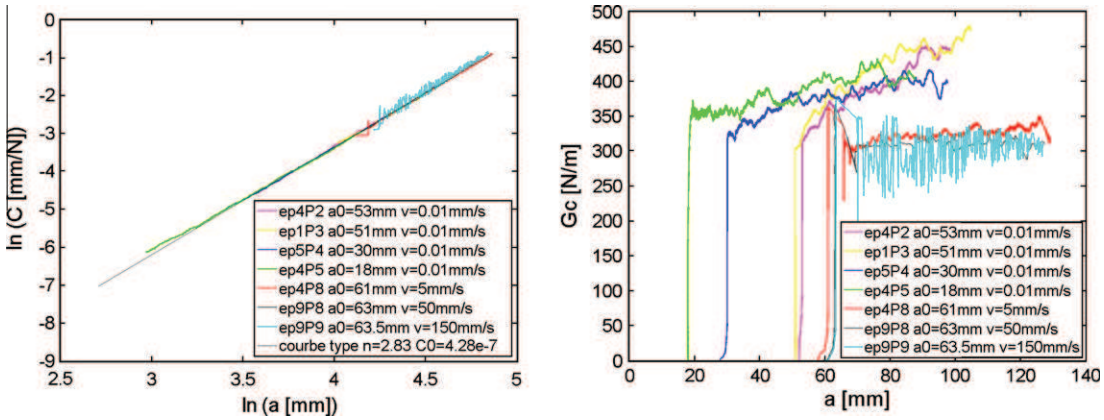

Fig. 3. T700/M21 compliance and resistance curves.

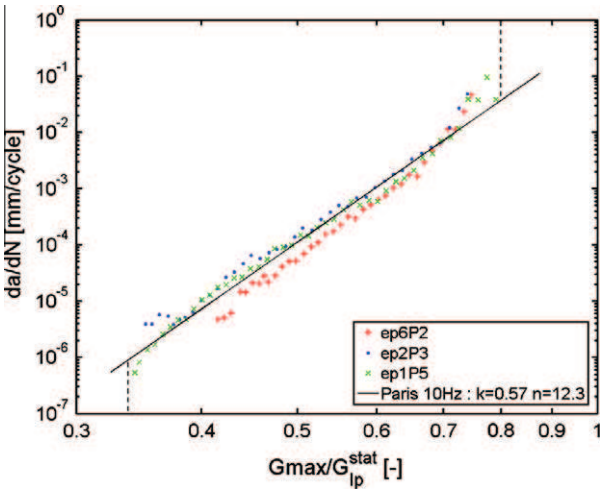

Fig. 5. Normalized Paris Law at 10 Hz and $R = 0.1$.

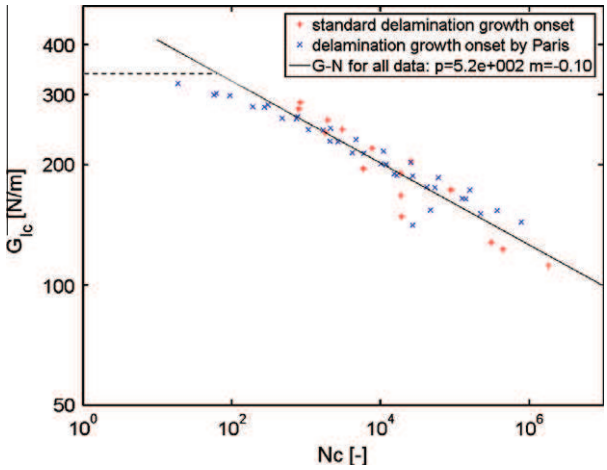

Fig. 7. *G–N* onset propagation curve standard and Paris method at 10 Hz and $R = 0.1$.

The total length of propagation is so divided into segments of length needed to increase the compliance of the specimen of 5% (Fig. 6a). For each first point of segment, the ERR is calculated with the compliance method (Eq. (3)). The number of cycles needed to propagate the delamination from the first point to the last point of the segment is then determined (Fig. 6b). This data are used to plot the *G–N* propagation curve point by point (Fig. 6c).

The delamination growth onset curve found is close to the one plotted with standard results (Fig. 7). The *G–N* propagation curve obtained by the Paris test process is then appropriate and saves a lot of test time. Considering the graph for the low number of cycles, the *G–N* curve deviates from the main slope for the highest ERR. Its intersection with the vertical axis illustrated by the dashed line represents an equivalent static ERR. This threshold value for one cycle between 300 N/m and 350 N/m is consistent with the static resistance curve (Fig. 3) and the Paris data (Fig. 5). On the other hand, the no propagation threshold does not appear on the *G–N* curve. In this propagation range the compliance variation is very small so the data reduction does not allow to represent it.

3. Dynamical fatigue test

3.1. Test conditions

3.1.1. System presentation

The dynamic tests use resonance and are conducted using a shaker. The device looks like an inertial tension–compression machine (Fig. 8).

The dynamic representation of the global system is a mass-spring system, where the specimen is represented by its opening stiffness (K_E). A spring (stiffness K_R) is connected in parallel with the specimen; the compression length of the spring ($\triangle l$) allows to fix the initial opening of the specimen (δ) which determines the average loading level (F_{mean}) (Part 3.2.1).

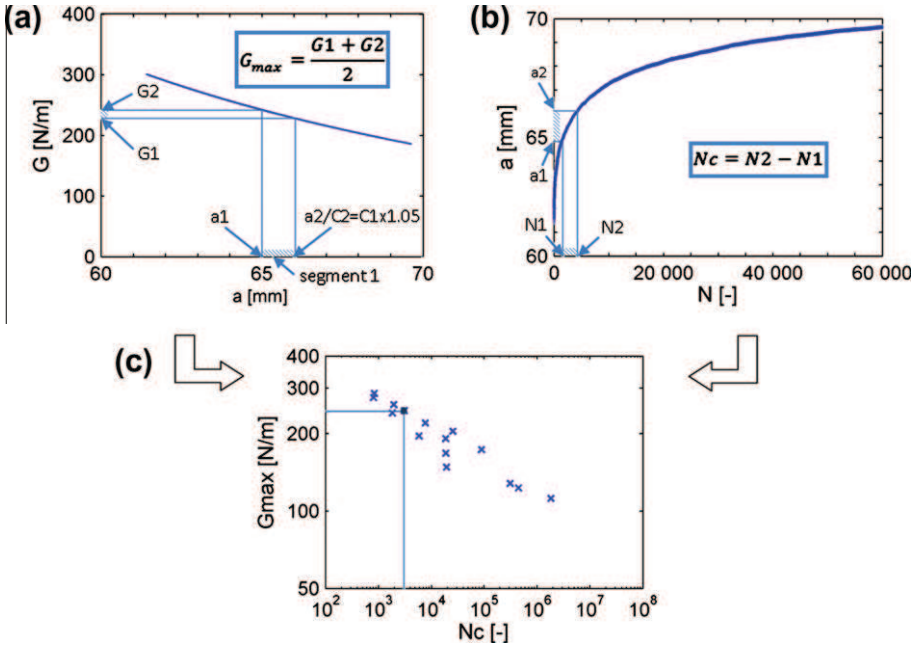

Fig. 6. Curve treatment to plot *G–N* curve.

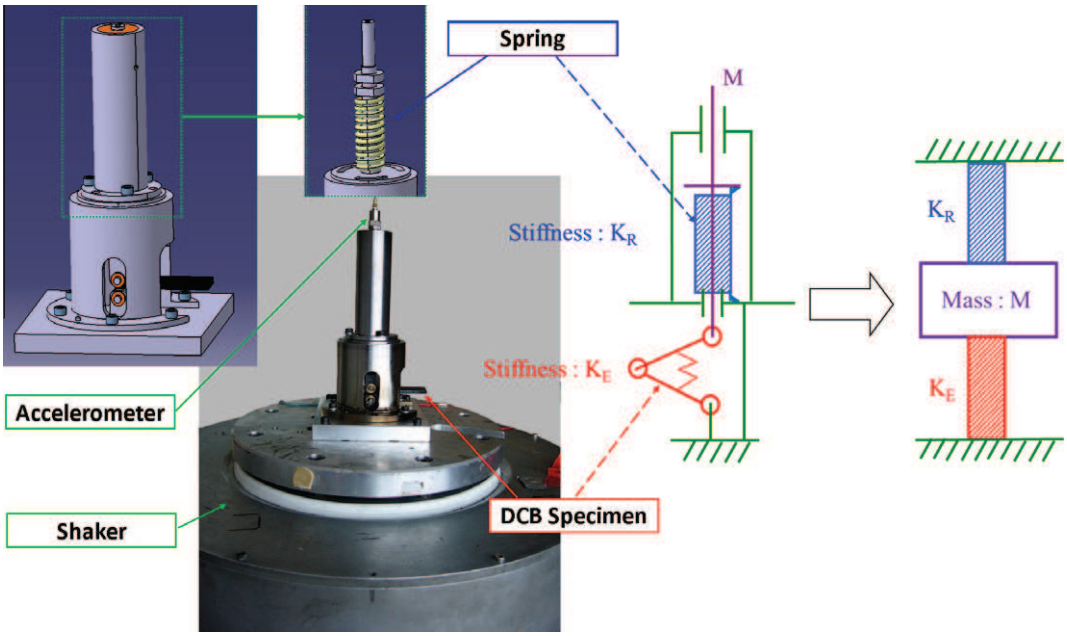

Fig. 8. Cinematic scheme of the mechanical test device.

During the experiment, the shaker generates a sinusoidal acceleration which sets the mass, M, in motion and thus loads the specimen around its equilibrium position. The loading frequency is chosen equal to the resonance frequency of the global system in order to take advantage of the amplification factor due to resonance.

The resonance frequency of the system depends on the mass, the specimen opening stiffness and the spring stiffness. The spring stiffness has to be lower than the specimen one to allow a precise opening adjustment. In order to obtain a high frequency, the mass has to be as light as possible and the opening stiffness as high as possible.

The cycling regulation at constant amplitude (F_{amp}) is performed by the control of the mass M acceleration (Part 3.2.2). (Fig. 9).

The load ratio R is completely determined by F_{mean} and F_{amp}:

$$R = \frac{F_{min}}{F_{max}} = \frac{F_{mean} - F_{amp}}{F_{mean} + F_{amp}} \tag{6}$$

Dynamical fatigue tests are performed at a controlled load ratio of $R = 0.1$ and at a frequency of 100 Hz (for the loading device and the specimen described below).

3.1.2. Dynamic specimen design

A specific specimen was designed for the dynamic tests. It is based on the standard DCB specimen. However to be adapted to the dynamic test constraints, the crack and the specimen lengths were modified ($L = 80$ mm, $b = 25$ mm, $h = 2.5$ mm and $a_0 = 30$ mm, Fig. 1). The dimensions of the loading blocks were the same as for the classical specimens. It was checked that the shortness of the initial crack length compared to the standard requirements does not necessitate any correction for the ERR calculation.

The first bending mode of the beam must not disturb the dynamics of the system, so this resonance mode was pushed above 100 Hz. Indeed, the specimen has to be as rigid as possible in bending: it was decided to keep a thickness of 5 mm, but the total length of the dynamical specimen was reduced to 80 mm in order to get a 1st mode up to 500 Hz.

As the opening stiffness of the specimen is strongly linked to the system resonance frequency, the initial crack size should be reduced to lead to the highest possible frequency for the system. But the Energy Restitution Rate (ERR) is very sensitive to the crack size which has to be precisely measured. To determine the specimen length, the ERR uncertainty was calculated based on measurement instrument precision and the adjustment of the initial opening. An initial crack length of 30 mm gives an acceptable compromise between stiffness and accuracy: $K_E = 150$ N/mm with an uncertainty lower than 20% for $G = 100$ N/m. To have a crack opening indicator, an electrical contactor was fixed at the end of the specimen (Fig. 10).

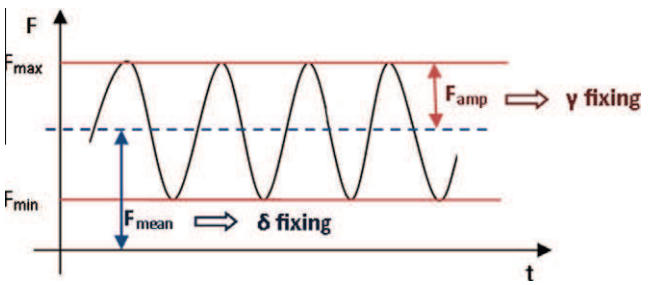

Fig. 9. Cycling definition.

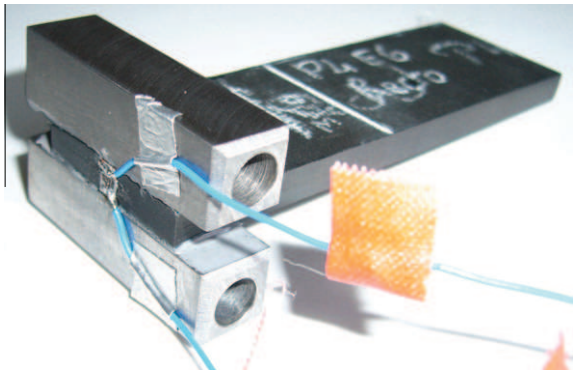

Fig. 10. Dynamical test specimen.

3.2. Experimental conditions and test procedure

3.2.1. Mean cycle fatigue loading value adjustment: F_{mean}

The adjustment of the initial position is described by the following equation (Fig. 8):

$$F_{moy} = K_E \cdot \delta = -M \cdot g - K_R \cdot \Delta l \tag{7}$$

As the principal axis is rigidly linked to the specimen, the crack opening δ imposed on the specimen is measured with the help of a displacement laser sensor pointed at the top surface of this axis (Fig. 11). The opening measurement begins as soon as the opening contactor is activated (see also 10). This initial equilibrium position is fixed with a lock nut.

3.2.2. Cycle fatigue loading amplitude adjustment: F_{amp}

System dynamics. The damped system dynamics without loading is described as follows:

$$M\ddot{u_m} + C\dot{u_m} + K_t u_m = 0 \tag{8}$$

$$\ddot{u_m} + 2\xi_r \omega_r \dot{u_m} + \omega_r^2 u_m = 0 \tag{9}$$

With u_m the mass displacement, $K_t = K_E + K_R$ the equivalent spring stiffness and ξ_r the reduced damping like:

$$\xi_r = \frac{C}{2\sqrt{K_t M}} \ll 1 \tag{10}$$

and ω_r like:

$$\omega_r = 2\pi f_r \tag{11}$$

With f_r the resonance frequency of the system.

The natural pseudo angular frequency of the system is then:

$$\varpi_r = \omega_r \sqrt{1 - \xi_r^2} \approx \omega_r = \sqrt{\frac{K_t}{M}} \tag{12}$$

The global system dynamics subject to the shaker acceleration are then governed by the following equation:

$$M\ddot{u} + C\dot{u} + K_t u = -M \cdot \ddot{u_p} \tag{13}$$

with u the mass displacement relative to the and u_p the shaker displacement.

Placing this in the Laplace domain:

$$U(\omega^2 M + i\omega C + K_t) = \omega^2 M \cdot U_p \tag{14}$$

with ω the angular frequency of the system excitation.

The transfer function of the system acceleration is:

$$H(\omega) = \frac{\ddot{U}}{U_p} = \frac{\omega^2 M}{-\omega^2 M + i\omega C + K_t} = \frac{\left(\frac{\omega}{\omega_r}\right)^2}{1 + 2i\xi_r \frac{\omega}{\omega_r} - \left(\frac{\omega}{\omega_r}\right)^2} \tag{15}$$

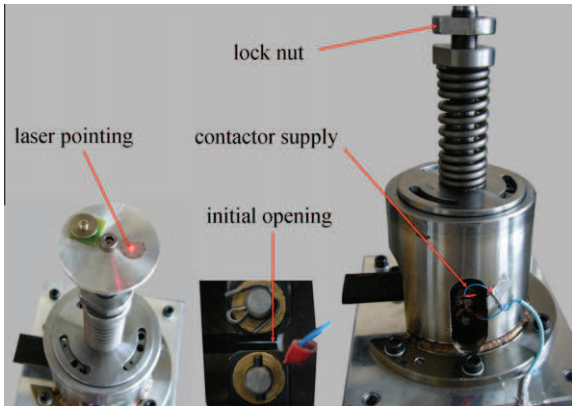

Fig. 11. Equilibrium position adjustment.

From this equation are taken:

- the absolute value of the amplification factor of the mass relative to the shaker, and
- the phase (ϕ) which at the resonant frequency is equal to $\phi_r = -90°$

A frequency sweeping test is therefore necessary to determine the resonant frequency of the global system and the amplification factor associated with it. This allows to calculate the acceleration value needed to control the shaker in order to get the desired acceleration of the mass.

F_{amp} Control.

The mass displacement is deduced from its acceleration:

$$\begin{cases} \ddot{u} = \gamma.sin(\omega \cdot t + \phi) \\ u = -\frac{\gamma}{\omega^2} sin(\omega \cdot t + \phi) \end{cases} \tag{16}$$

The load applied on the specimen is:

$$\begin{aligned} F_{amp} \cdot sin(\omega \cdot t + \phi) &= -K_E \cdot u = K_E \frac{\gamma}{\omega^2} sin(\omega \cdot t + \phi) \\ &= K_E \frac{|H(\omega)|\gamma_p}{\omega^2} sin(\omega \cdot t + \phi) \end{aligned} \tag{17}$$

It was decided to directly control the mass acceleration amplitude, M (γ), instead of the amplitude of the shaker acceleration (γ_p) which is usually the case. This has the advantage of avoiding any accurate measurement of the system transfer function, the mass-spring-specimen, which revealed a bit delicate to achieve. Indeed it is sensitive to the sweeping speed, and friction caused by the guiding rails leads to some difficulties in the very low range of imposed acceleration. The amplitude of acceleration γ_c is then imposed during loading and results in an accurate value for the load on the DCB specimen (Eq. (18)).

$$F_{amp} = K_E \frac{\gamma_c}{\omega^2} \tag{18}$$

3.2.3. Operating conditions in fatigue

The fatigue test to determine the threshold for crack propagation must be performed at a fixed load level and a given load ratio R (Fig. 9). Firstly the average load level on the specimen F_{mean} is completely defined by the initial load imposed by the spring (Part 3.2.1). Indeed it is not modified by the specimen stiffness change when the delamination propagates during the fatigue test. Secondly in order to fix the load ratio during the fatigue test, F_{amp} has to be kept constant (Eq. (6)). These conditions must be held during the propagation of the crack until the defined stopping criterion is reached.

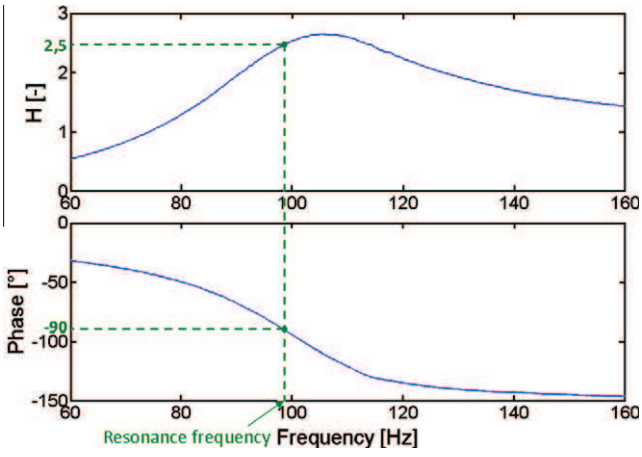

Fig. 12. Experimental system transfer function.

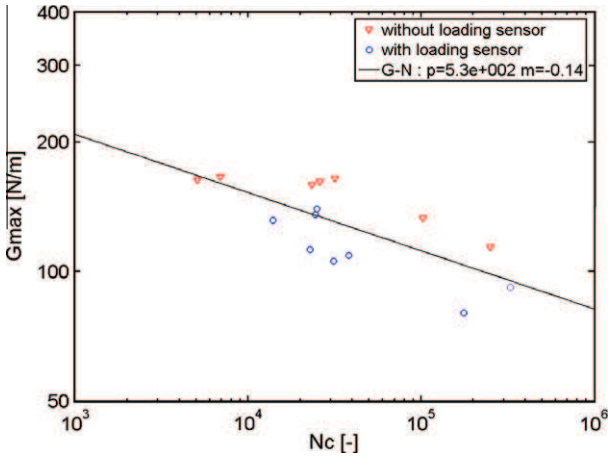

Fig. 13. *G–N* curve at 100 Hz with and without the load sensor.

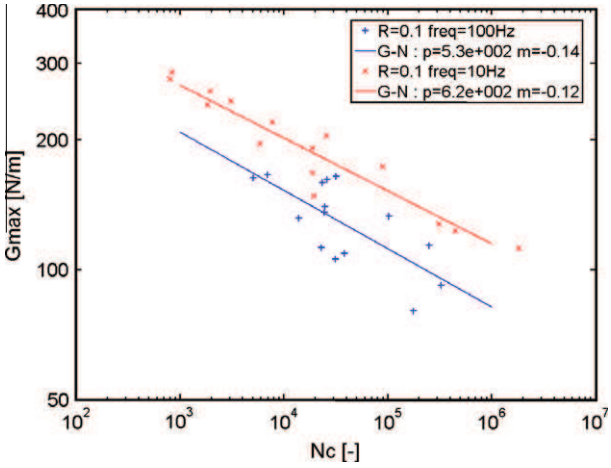

Fig. 14. *G–N* propagation curve: 10 Hz and 100 Hz.

It was decided to follow the evolution of the resonant frequency during the fatigue test; it has two advantages when the crack propagates.

- It allows to follow the crack progress and to define a test stopping criterion.
  When the delamination crack propagates, the opening stiffness of specimen decreases with the resonance frequency [24]. The curve of the transfer function is shifted to lower frequencies.
  If the loading was performed at fixed frequency, the amplification factor would also decrease (Fig. 12). Thus, as the test is controlled by the relative acceleration of the mass, the acceleration imposed by the shaker should increase to meet γ_c. This increase of input acceleration would be the unique indicator of the progress of the crack which would be difficult to quantify precisely.
  For a loading which follows the resonant frequency, the input frequency adapts to lock itself to the resonant frequency by keeping the phase of the transfer function equal to $-90°$ (Part 3.2.2). The change in input frequency is then directly linked to the change in stiffness of the specimen; and this later very easily linked to the crack extension through the compliance law (Fig. 3). The stopping frequency of the test is calculated to get a stiffness reduction of the specimen of about 5% as it is recommended in the standard fatigue test [3]. In this study the frequency shift is around 1.5 Hz corresponding to a propagation of 0.5 mm for the test specimens.
- It compensates the reduction in stiffness to keep F_{amp} almost constant
  When the delamination propagates, the opening specimen stiffness K_E and the resonant frequency ω_r decreases in the expression of F_{amp} (Eq. (18)). But this resonant frequency is changing with K_E and so it comes at the resonance that:

$$F_{amp} = K_E \frac{\gamma_c}{\omega_r^2} = \frac{K_E}{K_t} M \cdot \gamma_c = \frac{K_E}{K_E + K_R} M \cdot \gamma_c \tag{19}$$

The reduction in stiffness is then largely compensated. To strictly obtain a constant F_{amp}, γ_c should be adapted as well. But it reveals

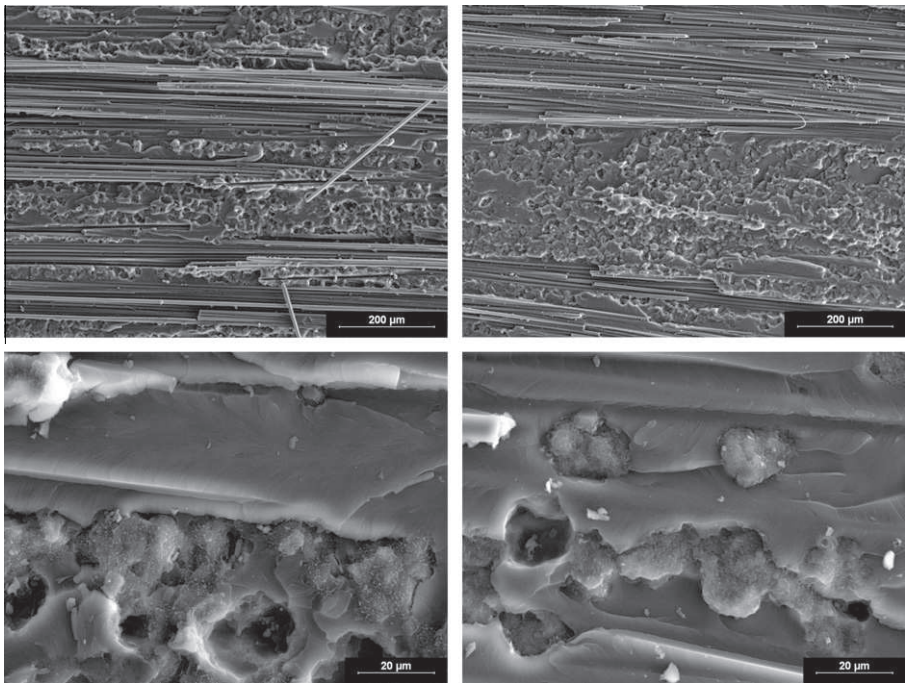

Fig. 15. SEM fracture surfaces for 10 Hz and 100 Hz (from left to right).

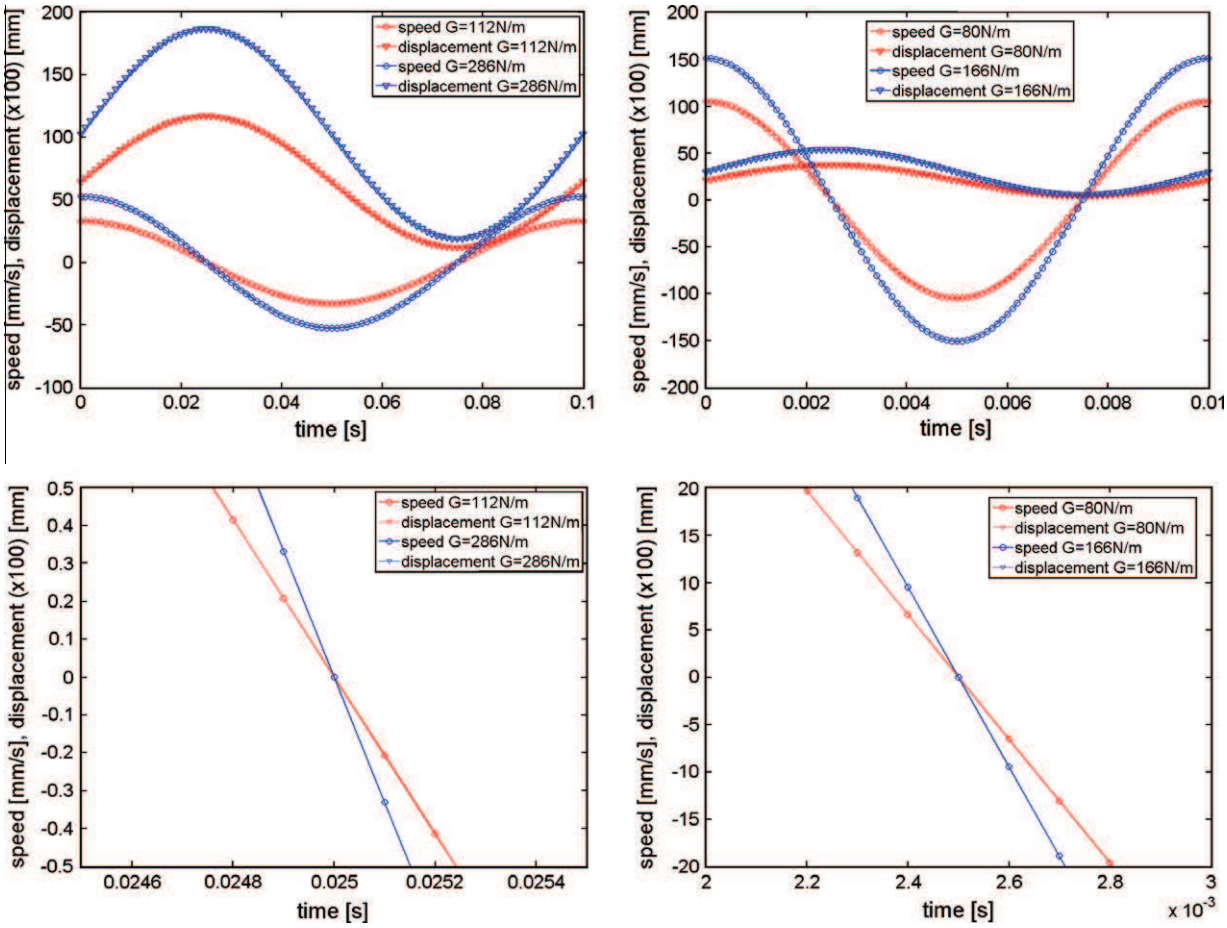

Fig. 16. One cycle opening displacement and speed for 10 Hz and 100 Hz (from left to right).

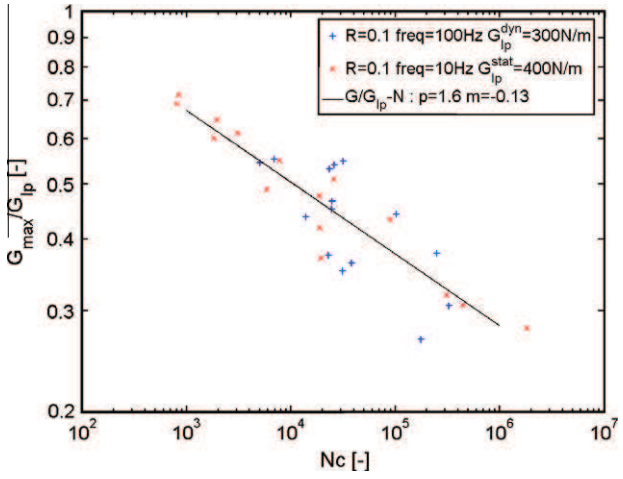

Fig. 17. *G–N* propagation curve on G_{Ip} : 10*Hz* and 100 Hz.

to be complex to set up for a limited accuracy gain. Indeed, without any adjustment of γ_c, this leads to less than 1% of error for F_{amp}.

3.2.4. Test facilities and operating process

The tests were performed on a shaker ($F_{max} = 40$ kN in sinus) of the DGA Techniques Aeronautiques test center. Two accelerometers were used to track accelerations of the mass and shaker. A voltage subtractor was used to measure the relative acceleration of the mass compared with the shaker which is the parameter controlled during tests γ_c. The data recorded during the test were: the amplitude of the relative acceleration of the mass and the frequency. The crack propagation was followed through the monitoring of the resonance frequency of the system. As seen before this frequency is linked to the opening stiffness of the specimen and then by the compliance law to the delamination size. In order to evaluate the specimen self-heat generation, specimen temperature evolutions were monitored with a thermal middle wavelength camera (sensitivity between 3 and 5 μm) on the entire sample and also near the crack tip.

The tests were thus controlled by setting the relative acceleration of the mass M at a constant value while following the resonant frequency of the system.

Once the initial opening was set, a frequency sweep was carried out at low acceleration to measure the resonant frequency of the global system and the amplification factor. Knowing the size of the initial crack and thus the specimen's initial stiffness, the apparent mass set in motion by the system was precisely calculated (this mass partially depends on the installation conditions). The acceleration γ_c necessary to impose the desired loading was then calculated (Eq. (19)). The minimum acceleration required to be imposed to the shaker was determined with the amplification factor and ensured γ_c to be obtained.

The fatigue test was then run and stopped when the final frequency was reached (Part 3.2.3). As for the classical tests, the data recorded during test were used to plot the *G–N* propagation curve with the ERR calculation compliance method (Eq. (3), Part 2.3.2).

For some specimens, the dynamic test device was improved by adding a piezoelectric load sensor under the loading axis. The zero sensor was adjusted before setting the specimen. F_{mean} and F_{amp} were then controlled using the sensor information which quite

simplify the process. As shown in the Fig. 13, both experimental results are in good agreement.

3.3. Results comparison

3.3.1. Frequency effect

The results are presented in the form of *G–N* curve to compare the fatigue propagation growth onset. Indeed, this data reduction is more suitable for dynamical test since a delamination propagation lead to a shift in frequency. So Paris tests cannot be performed for a long range of crack propagation when assuming a constant frequency.

The propagation thresholds obtained from the tests at 100 Hz are lower than those found at 10 Hz (Fig. 14). As the frequency increases, the strength of the material to crack propagation seems to decrease. Temperature specimen evolution due to vibrations at 100 Hz was monitored during fatigue and did not show significant heating of the material (relative change of temperature below 1 °C at the crack tip). So the behavior difference between the two frequencies cannot be explained by a temperature increase. The frequency effect seems more likely to be linked with a loading rate effect [16]: when loading at 100 Hz the strain rate applied to the material is greater than for 10 Hz. This strain rate rise can explain the decrease in fatigue crack growth resistance [23,25].

The SEM fracture surfaces of 10 Hz specimen and 100 Hz specimen are rather similar (Fig. 15 top). Many thermoplastic nodules added to increase the composite matrix toughness are distinctly observed for the largest magnification. The only tiny difference between specimen takes place in the thermoplastic nodules fracture surface, which seem to present plastic deformation (white tips on the nodule surface) for the 10 Hz specimens (Fig. 15 bottom-left) whereas the 100 Hz specimens nodules have a matt aspect (Fig. 15 bottom-right). This might be associated with the material rate dependency reported in part 2.2.

3.3.2. Strain rate effect

During the cycling the specimen opening displacement and speed are in phase quadrature: when the displacement is maximal the speed is equal to zero. In order to compare the two frequency tests, ERR and speed were plotted for the maximal and minimal ERR of the *G–N* curve ranges ($10\,\text{Hz} := [112\,\text{N/m}; 286\,\text{N/m}]$, $100\,\text{Hz} := [80\,\text{N/m}; 166\,\text{N/m}]$) (Fig. 16). The maximal displacement corresponds to the maximal ERR imposed in the cycle, that is where the fatigue cycling is the most efficient. The rates calculated around this ERR peak are greater for 100 Hz than for 10 Hz : $1\ e^{-4}$ second before the maximal displacement, the opening speeds for 10 Hz tests are between 0.207 mm/s and 0.331 mm/s whereas the ones for 100 Hz tests range between 6.58 mm/s and 9.48 mm/s.

To take into consideration the material rate dependency (Part 2.2), the ERR used for plotting the *G–N* curve is adimensioned by $G_{f_p^{stat}}$ in the 10 Hz test case and by $G_{f_p^{dyn}}$ in the 100 Hz one (Fig. 17). The two *G–N* curves are similar which confirms that this frequency effect is linked to a rate effect. The fatigue delamination growth onset of a material can then be determined with the new test in resonance taking into consideration this rate effect. The main *G–N* curve characterizing the material in fatigue was found to follow a log-linear law:

$$\frac{G_{max}}{G_{Ip}} = 1.6 \times N_c^{-0.13} \tag{20}$$

4. Conclusions

A new dynamical fatigue test at resonance has been developed for propagation test in mode I. This system based on DCB specimen is a dynamic mass-spring-specimen that is designed to resonate. The defined methodology allows a reproducible stopping condition identical to standard tests that are performed at lower frequencies (10 Hz). For now the device sizing limits the resonant frequency of the system to around 100 Hz. This test frequency prevents from reaching gigacycle within a reasonable test duration. In order to obtain higher frequencies, the device should be improved by reducing the mass weight and the friction in the axis guide. Nevertheless, this system enabled to perform resonance DCB fatigue test at high frequency without heat generation (no more than 1 °C) and to proceed to the fatigue characterization of a laminate composite material.

As reference standard fatigue tests in mode I at 10 Hz were conducted to determine the Paris law and fatigue propagation growth onset curve (*G–N*). A new data reduction was settled to allow plotting a *G–N* curve with Paris results which matches with the standard one. Comparison of results between the tests at different frequencies highlighted a frequency effect which was found to be likely due to a rate effect. By using adimensional ERR values taking into consideration the distinct dynamical and static propagation ERR, *G–N* curves at both frequencies were unified (Eq. (20)). Then, the dynamical test method allows to obtain a trustworthy *G–N* curve by reducing the time taken by a factor of ten.

References

[1] Green PD. Current and future problems in structural acoustic fatigue. In: AGARD symposium, volume impact of acoustic loads on aircraft structures; 1994. p. 1.1–1.5.

[2] European Aviation Safety Agency. Proof of structure – fatigue and damage tolerance. In: AMC 20–29 composite aircraft, structure; 2010.

[3] ASTM-D6115. Standard test method for mode I fatigue delamination growth onset of unidirectional fiber-reinforced polymer matrix composite; 1997.

[4] Brunner AJ, Murphy N, Pinter G. Development of a standardized procedure for the characterization of interlaminar delamination propagation in advanced composites under fatigue mode I loading conditions. Eng Fracture Mech 2009;76(18):2678–89.

[5] Brunner AJ, Stelzer S, Pinter G, Terrasi GP. Mode II fatigue delamination resistance of advanced fiber-reinforced polymere matrix laminates: towards the development of a standardized test procedure. Int J Fatigue 2012. http://dx.doi.org/10.1016/j.ijfatigue.2012.02.021.

[6] Hojo Masaki, Ando Tadashi, Tanaka Mototsugu, Adachi Taiji, Ochiai Shojiro, Endo Yoshihiro. Modes I and II interlaminar fracture toughness and fatigue delamination of CF/epoxy laminates with self-same epoxy interleaf. Int J Fatigue 2006;28(10):1154–65.

[7] Arguelles A, Vina J, Canteli AF, Castrillo MA, Bonhomme J. Interlaminar crack initiation and growth rate in a carbon-fibre epoxy composite under mode-I fatigue loading. Compos Sci Technol 2008;68(12):2325–31.

[8] Sjogren A, Asp LE. Effects of temperature on delamination growth in a carbon/epoxy composite under fatigue loading. Int J Fatigue 2002;24(2–4):179–84.

[9] George TJ, Seidt J, Shen MHH, Nicholas T, Cross CJ. Development of a novel vibration-based fatigue testing methodology. Int J Fatigue 2004;26(5):477–86.

[10] Morrissey RJ, McDowell DL, Nicholas T. Frequency and stress ratio effects in high cycle fatigue of Ti–6Al–4V. Int J Fatigue 1999;21(7):679–85.

[11] Bathias Claude. Piezoelectric fatigue testing machines and devices. Int J Fatigue 2006;28(11):1438–45.

[12] Xue HQ, Tao H, Monternbault F, Wang QY, Bathias C. Development of a three-point bending fatigue testing methodology at 20 kHz frequency. Int J Fatigue 2007;29:2085–93.

[13] Marines I, Dominguez G, Baudry G, Vittori JF, Rathery S, Doucet JP, Bathias C. Ultrasonic fatigue tests on bearing steel AISI-SAE 52100 at frequency of 20 and 30 kHz. Int J Fatigue 2003;25:1037–46.

[14] Sohar CR, Betzwar-Kotas A, Gierl C, Weiss B, Danninger H. Gigacycle fatigue behavior of a high chromium alloyed cold work tool steel. Int J Fatigue 2008;30(7):1137–49.

[15] Wang QY, Li T, Zeng XG. Gigacycle fatigue behavior of high strength aluminum alloys. Procedia Eng: Fatigue 2010;2(1):65–70.

[16] Sims GD. Fatigue test methods, problems and standards. In: Harris Bryan, editor. Fatigue in composites. CRC Press; 2003 [p. 36–62, chapter 2].

[17] Xiao XR, Al-Hmouz I. Effect of load frequency on the tensile fatigue behavior of angle-ply AS4/PEEK. In: The 11th international conference on composite materials; 1997. p. 124–34.

[18] Wang QY, Sriraman MR, Kawagoishi N, Chen Q. Fatigue crack growth of bonded composite repairs in gigacycle regime. Int J Fatigue 2006;28(10):1197–201.

[19] Michel SA, Kieselbach R, Martens HJ. Fatigue strength of carbon fibre composites up to the gigacycle regime (gigacycle-composites). Int J Fatigue 2006;28(3):261–70.

[20] Hosoi A, Sato N, Kusumoto Y, Fujiwara K, Kawada H. High-cycle fatigue characteristics of quasi-isotropic CFRP laminates over 10^8 cycles (initiation and propagation of delamination considering interaction with transverse cracks). Int J Fatigue 2010;32(1):29–36.
[21] Hosoi A, Yagi S, Nagata K, Kawada H. Interaction between transverse cracks and edge delamination considering free-edge effects in composite laminates. In: 16th International conference on composite materials; 2007.
[22] ASTM-D5528, Standard test method for mode I interlaminar fracture toughness of unidirectional fiber-reinforced polymer matrix composite; 1994.
[23] Kusaka T, Hojo M, Mai YW, Kurokawa T, Nojima T, Ochiai S. Rate dependence of mode I fracture behaviour in carbon-fibre/epoxy composite laminates. Compos Sci Technol 1998;58(3–4):591–602.
[24] Saravanos DA, Hopkins DA. Effects of delaminations on the damped dynamic characteristics of composite laminates: analysis and experiments. J Sound Vib 1996;192(5):977–93.
[25] Pascault JP, Sautereau H, Verdu J, Williams RJJ. Yielding and fracture of polymer network. Volume 64 of thermosetting polymers. Plastics Engineering. New York: CRC Press; 2002. p. 350–88.